MULTI-FRAME SUPER-RESOLUTION MRI USING COUPLED LOW-RANK TUCKER APPROXIMATION

Clémence Prévost, F Odille

▶ **To cite this version:**

Clémence Prévost, F Odille. MULTI-FRAME SUPER-RESOLUTION MRI USING COUPLED LOW-RANK TUCKER APPROXIMATION. 2022. hal-03617754

HAL Id: hal-03617754
https://hal.science/hal-03617754

Preprint submitted on 23 Mar 2022

HAL is a multi-disciplinary open access archive for the deposit and dissemination of scientific research documents, whether they are published or not. The documents may come from teaching and research institutions in France or abroad, or from public or private research centers.

L'archive ouverte pluridisciplinaire **HAL**, est destinée au dépôt et à la diffusion de documents scientifiques de niveau recherche, publiés ou non, émanant des établissements d'enseignement et de recherche français ou étrangers, des laboratoires publics ou privés.

MULTI-FRAME SUPER-RESOLUTION MRI USING COUPLED LOW-RANK TUCKER APPROXIMATION

C. Prévost[1], *F. Odille*[2,3]

[1]Univ. Lille, CNRS, Centrale Lille, UMR 9189 CRIStAL, F-59000 Lille, France
[2]Inserm, Université de Lorraine, U1254 IADI, F-54000 Nancy, France
[3]Inserm, Université de Lorraine, CHRU Nancy, CIC-IT 1433, F-54000 Nancy, France

ABSTRACT

In this paper, we address the multi-frame super-resolution MRI problem. We formulate the reconstruction problem as a coupled tensor multilinear approximation. We prove that exact recovery of the high-resolution 3D isotropic image is achievable for a variety of multilinear ranks. We propose a simple algorithm based on Tikhonov regularization to perform the reconstruction. Our simulations on real datasets illustrates the good performance of the proposed approach, with a lower computation time than state-of-the-art methods.

1. INTRODUCTION

Magnetic resonance imaging (MRI) is a versatile medical imaging modality, providing excellent contrast between soft tissues. The acquisition parameters can indeed be tuned in order to make this contrast sensitive to various tissue properties, such as proton density, and longitudinal and transverse relaxation times (respectively T_1 and T_2). MRI acquisition consists of repeatedly exciting protons in the human body, using various electromagnetic pulses, and acquiring a small amount of Fourier samples from the image.

Typical MRI data consist in 2D or 3D images in arbitrary orientations. The latter possess two in-plane spatial dimensions and a third spatial slice dimension, hence they can be seen as tensors. However, 3D MRI suffers from a relatively slow acquisition time, typically on the order of minutes. To circumvent this drawback, super-resolution techniques have been shown to be efficient in a number of situations [1, 2, 3]. They consist in recovering a 3D high-resolution image from one or several low-resolution observations.

Recently, it has been proposed to recover the high-resolution image from a single low-resolution observation using deep learning [4, 5]. However, in the presence of small lesions, it may be preferable to consider several observations for diagnostic use of the images and to avoid relying on an external patient database for the prior. Therefore, in the remainder, we will focus on super-resolution from multiple observations, also termed multi-frame super-resolution.

This work was partly supported by the ANR project "Chaire IA Sherlock" ANR-20-CHIA-0031-01 hold by P. Chainais, as well as by the national support within the *programme d'investissements d'avenir* ANR-16-IDEX-0004 ULNE and Région HDF.

Multi-frame super-resolution MRI consists of acquiring several complementary observations of the organ of interest, e.g. three orthogonal scans [6], or three scans with sub-voxel shifts in the slice direction [7]. Each observation has high in-plane resolutions (1 mm or less) in the first two dimensions, and low resolution in the slice direction (typically 3 to 10 mm). The acquisition process can be modelled, including a blurring/downsampling operator in the slice direction, Patient motion is dealt with as a pre-processing step using motion-compensated reconstruction [8] and/or image registration [9].

The super-resolution problem is often solved by regularized inversion. Besides Tikhonov regularization [10], total variation [11] or Beltrami energy regularizers [8] have been proposed, as well as constraints on the rank of the matricized image (this method was applied to single-frame super-resolution) [12], and patch-based regularization methods [13]. The last two methods are intended to exploit the low-rank structure of the images. Iterative solvers are used in all these cases, such as the conjugate gradient (Tikhonov), primal dual gradient descent (Beltrami) or the alternating direction method of multipliers (low-rank and patch-based methods).

However, matrix patch-based methods possess a high computational burden, as they require many operations for extracting patches from the image, sorting them, and performing dimensionality reduction. They also fail at preserving the natural tensor shape of the observations. More importantly, no theoretical guarantees for exact reconstruction of the high-resolution images were provided.

Tensor-based reconstruction methods were recently envisioned in some engineering fields such as remote sensing of spectrum cartography [14, 15, 16]. In the field of medical imaging, coupled tensor models were used for the reconstruction of dynamic cardiac images [17] of functional MRI reconstruction [18], for instance. Such approaches preserved the structural information between the dimensions of the images. Theoretical guarantees for exact image recovery were formulated also formulated.

Several low-rank factorizations can be considered for approximating tensor data. The multilinear (also known as Tucker) factorization was considered in [15] with an application in remote sensing. A closed-form SVD-based algorithm was proposed. The approach of [15] considered 3D image reconstruction from two degraded tensors.

In this paper, we propose a novel tensor-based approach for multi-frame super-resolution MRI. The proposed approach is based on a coupled low-rank multilinear approximation of three MRI observations. We introduce an algorithm with low computational burden, named isometRic Image Reconstruction by COupled Tensor Tucker Approximation (RICOTTA), that is inspired by the higher-order SVD [19]. We prove that our approach achieves exact reconstruction of the high-resolution image for a variety of multilinear ranks. We illustrate the performance of our method on a set of real datasets. We show that our algorithm yields good reconstruction, with lower computation time than matrix-based super-resolution methods.

Notation– We mainly follow the notations of [20, 21]. We use lowercase (a) or uppercase (A) plain font for scalars, boldface lowercase ($\boldsymbol{a}$) for vectors, uppercase boldface ($\mathbf{A}$) for matrices, and calligraphic ($\boldsymbol{\mathcal{A}}$) for tensors. The elements of vectors/matrices/tensors are accessed as a_i, $A_{i,j}$ and $\mathcal{A}_{i_1,\ldots,i_N}$ respectively.

For a matrix $\mathbf{A}$, we denote its transpose and Moore-Penrose pseudoinverse as $\mathbf{A}^\mathsf{T}$ and $\mathbf{A}^\dagger$ respectively. The notation $\mathbf{I}_M$ is used for the $M \times M$ identity matrix and $\mathbf{0}_{L\times K}$ for the $L \times K$ matrix of zeroes. We use the symbol $\boxtimes$, $\otimes$ and $\odot$ for the Kronecker, tensor and Khatri-Rao products, respectively. We also denote by $\text{tSVD}_R(\mathbf{X}) \in \mathbb{R}^{n\times R}$ a matrix containing R leading right singular vectors of $\mathbf{X}$.

We use $\text{vec}\{\cdot\}$ for the standard column-major vectorization of a tensor or a matrix. Operator $\bullet_p$ denotes contraction on the pth index of a tensor, e.g., $[\boldsymbol{\mathcal{A}} \bullet_1 \mathbf{M}]_{ijk} = \sum_\ell \mathcal{A}_{\ell jk} M_{i\ell}$. For a tensor $\boldsymbol{\mathcal{Y}} \in \mathbb{R}^{I\times J\times K}$, its first unfolding is denoted by $\mathbf{Y}^{(1)} \in \mathbb{R}^{JK\times I}$. The following shorthand notation is used for the multilinear product: $[\![\boldsymbol{\mathcal{G}}; \mathbf{U}, \mathbf{V}, \mathbf{W}]\!] = \boldsymbol{\mathcal{G}} \bullet_1 \mathbf{U} \bullet_2 \mathbf{V} \bullet_3 \mathbf{W}$.

2. SUPER-RESOLUTION BY COUPLED MULTILINEAR APPROXIMATION

2.1. The image reconstruction problem

We aim at recovering a high-resolution 3D isotropic (in this context, an image is said isotropic if its dimensions are all equal) image (HRII) with high resolutions. It can be viewed as a tensor $\boldsymbol{\mathcal{Z}} \in \mathbb{R}^{I\times J\times K}$, where K represents the number of frontal slices and I and J stand for the in-plane resolutions.

We observe three pre-processed low-resolution 3D images (LRI) available, that can be viewed as degraded versions of $\boldsymbol{\mathcal{Z}}$. The observations are denoted to as $\boldsymbol{\mathcal{Y}}_1 \in \mathbb{R}^{I_1\times J\times K}$, $\boldsymbol{\mathcal{Y}}_2 \in \mathbb{R}^{I\times J_2\times K}$ and $\boldsymbol{\mathcal{Y}}_3 \in \mathbb{R}^{I\times J\times K_3}$, respectively. The dimensions I_1, J_2 and K_3 stand for the degraded dimensions, *i.e.*, $I_1 \ll I$, $J_2 \ll J$ and $K_3 \ll K$, respectively.

Formally, we can express the degradation model as mode product of the HRII $\boldsymbol{\mathcal{Z}}$ with some degradation matrices as

$$\begin{cases} \boldsymbol{\mathcal{Y}}_1 &= \boldsymbol{\mathcal{Z}} \bullet_1 \mathbf{D}_1 + \boldsymbol{\mathcal{E}}_1, \\ \boldsymbol{\mathcal{Y}}_2 &= \boldsymbol{\mathcal{Z}} \bullet_2 \mathbf{D}_2 + \boldsymbol{\mathcal{E}}_2, \\ \boldsymbol{\mathcal{Y}}_3 &= \boldsymbol{\mathcal{Z}} \bullet_3 \mathbf{D}_3 + \boldsymbol{\mathcal{E}}_3. \end{cases} \tag{1}$$

The degradation matrices $\mathbf{D}_i$ ($i = 1, 2, 3$) are downsampling matrices such as $\mathbf{D}_1 \in \mathbb{R}^{I_1\times I}$, $\mathbf{D}_2 \in \mathbb{R}^{J_2\times J}$ and $\mathbf{D}_3 \in \mathbb{R}^{K_3\times K}$ and depend on the sensor specificities. The tensors $\boldsymbol{\mathcal{E}}_i$ ($i = 1, 2, 3$) represent white Gaussian noise terms.

A possible way to formulate the image reconstruction problem is to consider the following optimization problem

$$\begin{aligned} \min_{\widehat{\boldsymbol{\mathcal{Z}}}} \lambda_1 \|\boldsymbol{\mathcal{Y}}_1 - \widehat{\boldsymbol{\mathcal{Z}}} \underset{1}{\bullet} \mathbf{D}_1\|_F^2 + \lambda_2 \|\boldsymbol{\mathcal{Y}}_2 - \widehat{\boldsymbol{\mathcal{Z}}} \underset{2}{\bullet} \mathbf{D}_2\|_F^2 \\ + \lambda_3 \|\boldsymbol{\mathcal{Y}}_3 - \widehat{\boldsymbol{\mathcal{Z}}} \underset{3}{\bullet} \mathbf{D}_3\|_F^2 + \mu \mathcal{R}(\widehat{\boldsymbol{\mathcal{Z}}}), \end{aligned} \tag{2}$$

where the scalars λ_i ($i = 1, 2, 3$) are balance parameters that control the weights of the LRI in the cost function. The operator $\mathcal{R}(\cdot)$ is a regularization operator and performs Tikhonov regularization [22] on the reconstructed HRII $\widehat{\boldsymbol{\mathcal{Z}}}$. Its weight is controlled by the user-specified scalar μ.

2.2. Coupled Tucker reformulation

In this paper, we propose to use a coupled tensor multilinear (Tucker) approximation to solve the reconstruction problem. We assume that the HRII $\boldsymbol{\mathcal{Z}}$ admits a Tucker decomposition with given multilinear ranks (R_1, R_2, R_3) as

$$\boldsymbol{\mathcal{Z}} = [\![\boldsymbol{\mathcal{G}}; \mathbf{U}, \mathbf{V}, \mathbf{W}]\!], \tag{3}$$

where $\mathbf{U} \in \mathbb{R}^{I\times R_1}$, $\mathbf{V} \in \mathbb{R}^{J\times R_2}$ and $\mathbf{W} \in \mathbb{R}^{K\times R_3}$ are the factor matrices and $\boldsymbol{\mathcal{G}} \in \mathbb{R}^{R_1\times R_2\times R_3}$ is the core tensor. Under this assumption, model (1) becomes

$$\begin{cases} \boldsymbol{\mathcal{Y}}_1 &= [\![\boldsymbol{\mathcal{G}}; \mathbf{D}_1\mathbf{U}, \mathbf{V}, \mathbf{W}]\!] + \boldsymbol{\mathcal{E}}_1, \\ \boldsymbol{\mathcal{Y}}_2 &= [\![\boldsymbol{\mathcal{G}}; \mathbf{U}, \mathbf{D}_2\mathbf{V}, \mathbf{W}]\!] + \boldsymbol{\mathcal{E}}_2, \\ \boldsymbol{\mathcal{Y}}_3 &= [\![\boldsymbol{\mathcal{G}}; \mathbf{U}, \mathbf{V}, \mathbf{D}_3\mathbf{W}]\!] + \boldsymbol{\mathcal{E}}_3. \end{cases} \tag{4}$$

Furthermore, solving (2) boils down to minimizing a cost function $\mathbf{f}_T(\widehat{\boldsymbol{\mathcal{G}}}, \widehat{\mathbf{U}}, \widehat{\mathbf{V}}, \widehat{\mathbf{W}})$ with respect to the low-rank factors $\mathbf{U}$, $\mathbf{V}$, $\mathbf{W}$, $\boldsymbol{\mathcal{G}}$. This cost function is such that

$$\begin{aligned} \mathbf{f}_T(\widehat{\boldsymbol{\mathcal{G}}}, \widehat{\mathbf{U}}, \widehat{\mathbf{V}}, \widehat{\mathbf{W}}) = \lambda_1 \|\boldsymbol{\mathcal{Y}}_1 - [\![\widehat{\boldsymbol{\mathcal{G}}}; \mathbf{D}_1\widehat{\mathbf{U}}, \widehat{\mathbf{V}}, \widehat{\mathbf{W}}]\!]\|_F^2 \\ + \lambda_2 \|\boldsymbol{\mathcal{Y}}_2 - [\![\widehat{\boldsymbol{\mathcal{G}}}; \widehat{\mathbf{U}}, \mathbf{D}_2\widehat{\mathbf{V}}, \widehat{\mathbf{W}}]\!]\|_F^2 \\ + \lambda_3 \|\boldsymbol{\mathcal{Y}}_3 - [\![\widehat{\boldsymbol{\mathcal{G}}}; \widehat{\mathbf{U}}, \widehat{\mathbf{V}}, \mathbf{D}_3\widehat{\mathbf{W}}]\!]\|_F^2 \\ + \mu \|[\![\widehat{\boldsymbol{\mathcal{G}}}; \widehat{\mathbf{U}}, \widehat{\mathbf{V}}, \widehat{\mathbf{W}}]\!]\|^2. \end{aligned} \tag{5}$$

2.3. Proposed algorithm

Rather than finding a local minimum of (5), we propose hereafter a closed-form algorithm as a sub-optimal solution for (4). This new approach is summarized in Algorithm 1, that we will further refer to as isometRic Image Reconstruction by COupled Tensor Tucker Approximation (RICOTTA).

Step 1 of RICOTTA estimates the matrix factors $\mathbf{U}$, $\mathbf{V}$, $\mathbf{W}$ by computing the truncated SVD (tSVD) of the concatenated unfoldings to ranks R_1, R_2, R_3, respectively. Step 2 of RICOTTA consists in solving the least-squares problem

$$\arg\min_{\widehat{\boldsymbol{\mathcal{G}}}} \|\mathbf{X}\,\text{vec}\{\widehat{\boldsymbol{\mathcal{G}}}\} - \boldsymbol{z}\|_F^2 + \mu \|\,\text{vec}\{\widehat{\boldsymbol{\mathcal{G}}}\}\|_F^2, \tag{6}$$

Algorithm 1: RICOTTA

input : $\mathcal{Y}_1, \mathcal{Y}_2, \mathcal{Y}_3, \mathbf{D}_1, \mathbf{D}_2, \mathbf{D}_3; R_1, R_2, R_3$

output: $\widehat{\mathcal{Y}} \in \mathbb{R}^{I \times J \times K}$

1. $\mathbf{U} \leftarrow \text{tSVD}_{R_1}\left(\left[\mathbf{Y}_2^{(1)}\ \mathbf{Y}_3^{(1)}\right]\right)$,
   $\mathbf{V} \leftarrow \text{tSVD}_{R_2}\left(\left[\mathbf{Y}_1^{(2)}\ \mathbf{Y}_3^{(2)}\right]\right)$,
   $\mathbf{W} \leftarrow \text{tSVD}_{R_3}\left(\left[\mathbf{Y}_1^{(3)}\ \mathbf{Y}_2^{(3)}\right]\right)$
2. $\widehat{\mathcal{G}} \leftarrow \underset{\mathcal{G}}{\text{argmin}}\ \mathbf{f}_T(\mathcal{G}, \widehat{\mathbf{U}}, \widehat{\mathbf{V}}, \widehat{\mathbf{W}})$;
3. $\widehat{\mathcal{Z}} = [\![\widehat{\mathcal{G}}; \widehat{\mathbf{U}}, \widehat{\mathbf{V}}, \widehat{\mathbf{W}}]\!]$.

which can be done through normal equations of the form

$$\left(\mathbf{X}^{\mathsf{T}}\mathbf{X} + \mu\mathbf{I}\right) \text{vec}\{\widehat{\mathcal{G}}\} = \mathbf{X}^{\mathsf{T}} \text{vec}\{z\}, \tag{7}$$

for which efficient solvers can be used [23]. Therefore, the total computational complexity of RICOTTA is

- $\mathcal{O}((R_1+R_2+R_3)IJK)$ flops for the truncated SVDs;
- $\mathcal{O}(\min(R_3^3+(R_1R_2)^3; R_1^3+(R_2R_3)^3))$ flops for solving the Sylvester equation in Step 2.

3. EXACT RECOVERY ANALYSIS

In this section, we provide gerenic guarantees for exact recovery of the HRII tensor in the noiseless case.

Theorem 3.1. *Assume that* $\mathbf{D}_1 \in \mathbb{R}^{I_1 \times I}$, $\mathbf{D}_2 \in \mathbb{R}^{J_2 \times J}$, *and* $\mathbf{D}_3 \in \mathbb{R}^{K_3 \times K}$ *are fixed full row-rank matrices. Let*

$$\mathcal{Z} = [\![\mathcal{G}; \mathbf{U}, \mathbf{V}, \mathbf{W}]\!], \tag{8}$$

where $\mathcal{G} \in \mathbb{R}^{R_1 \times R_2 \times R_3}$, $R_1 \leq I$, $R_2 \leq J$, $R_3 \leq K$, *and* $\mathbf{U} \in \mathbb{R}^{I \times R_1}$, $\mathbf{V} \in \mathbb{R}^{J \times R_2}$, $\mathbf{W} \in \mathbb{R}^{K \times R_3}$ *are random tensor and matrices, distributed according to an absolutely continuous probability distribution. We also assume that* $\mathcal{E}_i$ *(*$i = 1, 2, 3$*) in* (1).

1. If either $R_3 \leq K_3$ *or* $R_1 \leq I_1$ *or* $R_2 \leq J_2$, *and*

$$\begin{cases} R_1 \leq \min(R_3, K_3)R_2, \\ R_2 \leq \min(R_3, K_3)R_1 \\ R_3 \leq \min(R_1, I_1)\min(R_2, J_2), \end{cases} \tag{9}$$

then with probability 1 *there exists a unique tensor* $\widehat{\mathcal{Z}}$ *such that* $\widehat{\mathcal{Z}} \bullet_1 \mathbf{D}_1 = \mathcal{Y}_1$, $\widehat{\mathcal{Z}} \bullet_2 \mathbf{D}_2 = \mathcal{Y}_2$ *and* $\widehat{\mathcal{Z}} \bullet_3 \mathbf{D}_3 = \mathcal{Y}_3$.

2. If $(R_1, R_2, R_3) > (I_1, J_2, K_3)$, *then the reconstruction is non-unique, i.e. there exist an continuum of* $\widehat{\mathcal{Z}}$ *such that* $\widehat{\mathcal{Z}} \bullet_1 \mathbf{D}_1 = \mathcal{Y}_1$, $\widehat{\mathcal{Z}} \bullet_2 \mathbf{D}_2 = \mathcal{Y}_2$ *and* $\widehat{\mathcal{Z}} \bullet_3 \mathbf{D}_3 = \mathcal{Y}_3$*; in fact,* $\|\widehat{\mathcal{Z}} - \mathcal{Z}\|$ *can be arbitrary large.*

In Figure 1, we illustrate the statement of Theorem 3.1. The region (a) where the HRII is recoverable is pictured in green while the red region (b) corresponds to ranks for which the HRII is not recoverable exactly. The hatched area corresponds to cases in which the conditions (9) are not satisfied.

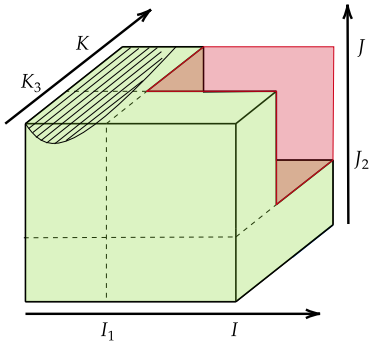

Fig. 1. Identifiability region depending on R_1, R_2 and R_3.

4. EXPERIMENTS

All simulations were run on a MacBook Pro with 2.3 GHz Intel Core i5 and 16GB RAM. The code was implemented in MATLAB. For basic tensor operations we used TensorLab 3.0 [24].

We compared the performance of RICOTTA to the multi-frame state-of-the-art [8]. Two super-resolution algorithms were considered. The first one used Tikhonov regularization and the second one used feature-preserving Beltrami regularization [25]. They will be further denoted to as SR-T and SR-B, respectively. They were tuned according to the original work [8]. In this paper, a preprocessing step was applied in order to cast the acquired data and observation model into the separable form given in (1).

To evaluate the quality of the reconstructed images $\widehat{\mathcal{Z}}$, we considered three quantitative metrics [26]. The first one was the peak signal to noise ratio (PSNR), defined as

$$\text{PSNR} = \frac{10}{K}\sum_{k=1}^{K} \log_{10}\left(\frac{IJE\{(\mathcal{Z})_{:,:,k}\}}{\|(\mathcal{Z})_{:,:,k} - (\widehat{\mathcal{Z}})_{:,:,k}\|_F^2}\right), \tag{10}$$

where $E\{\cdot\}$ denoted the expectation operator. The second metric was the Cross-Correlation (CC) [26]. The third one was the widely used sharpness index (SI) [27]. We computed the average SI across in-plane spatial dimensions ($\text{SI}_{1,2}$) and the average SI across the slice dimension (SI_3). We also showed the computational time for each algorithm, given by the `tic` and `toc` functions of MATLAB. The best results will be shown in bold in the following tables.

4.1. Data description

A test object (physical phantom), used for quality control and resolution assessment, was scanned with a 3T Prisma MRI scanner (Siemens Healthineers, Erlangen, Germany). First, a high-resolution image was obtained and was used as the ground truth for comparison of the different SR reconstruction methods. The acquisition used a turbo spin echo sequence to produce a groundtruth image (HRIII) $\mathcal{Z} \in \mathbb{R}^{224 \times 224 \times 224}$. The scan time for HRII was 6 min 30 s. The phantom LRI data were acquired with voxels of size

$1\times1\times8$ mm^3. The downsampling ratio between the HRII and the LRI was $d = 8$, yielding $\mathbf{D}_1 = \mathbf{D}_2 = \mathbf{D}_3 \in \mathbb{R}^{28\times224}$. The acquisition of each of the three LRI in that case took approximately 1 min.

The volunteer experiment was conducted on a 3T Signa HDxt MRI scanner (General Electric, Milwaukee, USA). The volunteer study was approved by an ethics committee and written informed consent was obtained (ClinicalTrials.gov identifier: NCT02887053). We acquired a HRII of the whole brain. The acquisition used a fast gradient echo sequence with a native resolution of $1 \times 1 \times 1$ mm^3 to produce a reference tensor $\boldsymbol{\mathcal{Z}} \in \mathbb{R}^{224\times224\times224}$. The scan time for HRII was 8 min. Brain LRI data were obtained with voxels of size $1 \times 1 \times 4$ mm^3 (downsampling ratio of 4). The acquisition of each LRI took approximately 2 min.

4.2. Performance for image reconstruction

For the physical phantom dataset, we ran RICOTTA with multilinear ranks $R = (220, 220, 30)$, weights $\lambda_1 = \lambda_2 = 1$ and λ_3 = 0.8 and $\mu = 0.02$. The reconstruction metrics were available in Table 1 and slices of the original and reconstructed HRII were displayed in Figure 2. RICOTTA yielded

Alg.	PSNR	CC	$SI_{1,2}$	SI_3	Time (s)
RICOTTA	**20.951**	**0.9633**	80.272	**429.720**	**11.966**
SR-T	18.091	0.9625	84.208	329.285	15.357
SR-B	19.808	0.9613	**95.801**	397.463	219.398

Table 1. Reconstruction for quality test phantom ($d = 8$).

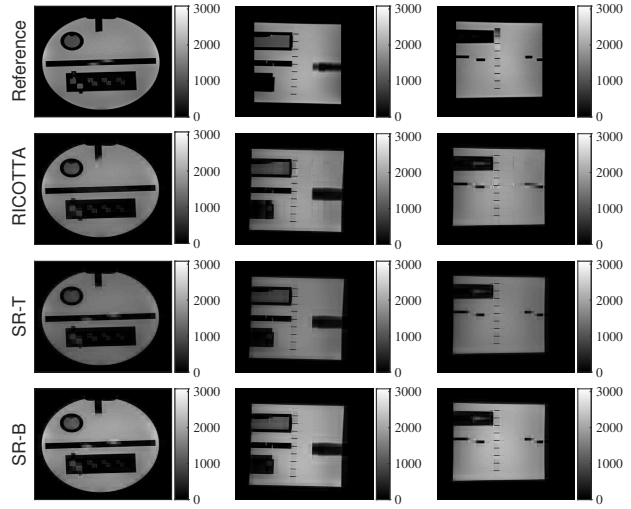

Fig. 2. Original and reconstructed slices of the HRII for quality test phantom ($d = 8$).

better PSNR, CC and SI in the frontal dimension compared to the SR-reconstruction method, but slightly lower SI in the plane dimensions. It had the lowest computation time for our implementation.

For the brain dataset, we ran RICOTTA with multilinear ranks $R = (220, 220, 50)$ and weights $\lambda_1 = \lambda_2 = 0.2$ and λ_3 = 0.8. We set the value of the regularization parametrer $\mu = 0.001$. The results were available in Table 2 and in Figure 3.

Alg.	PSNR	CC	$SI_{1,2}$	SI_3	Time (s)
RICOTTA	**24.764**	**0.9153**	174.346	**580.933**	**236.506**
SR-T	22.557	0.8854	**278.068**	422.824	266.280
SR-B	22.709	0.8842	264.000	447.629	361.398

Table 2. Reconstruction for brain dataset ($d = 4$).

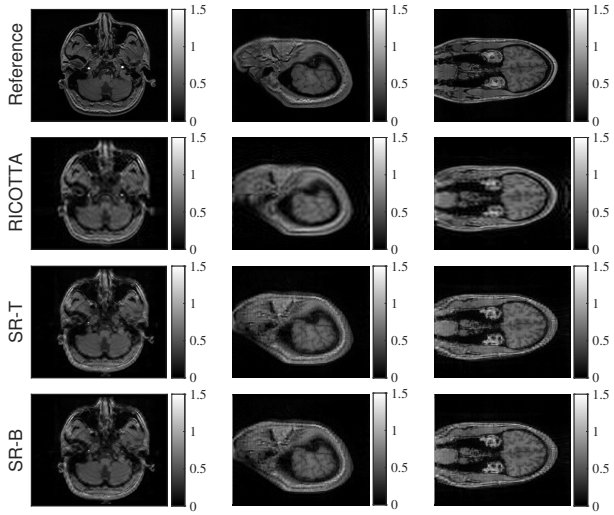

Fig. 3. Original and reconstructed slices of the HRII for real brain data ($d = 4$).

The proposed algorithm provided better PSNR and CC than the state-of-the-art. In particular, the SI in the frontal dimension was way higher than that provided by the SR algorithms. RICOTTA had the lowest computation time. However, the in-plane sharpness index was the lowest.

5. CONCLUSION

In this paper, we proposed a novel tensor method for reconstructing MRI high-resolution 3D volumes. The proposed algorithm achieves exact reconstruction for a variety of multilinear ranks. Our simulations on real data shows that RICOTTA performs good reconstruction with a competitive time. We hope that this work opens new perspectives on using tensor factorization in medical imaging applications. The proposed method should be applicable to a wide range of MRI acquisition techniques. It could help improve the trade-off between scan time, resolution, SNR and contrast in MRI. Still several questions remain open, such as the choice of the model parameters. Different regularization operators can be envisioned, such as Beltrami regularization. These matters will be investigated in future works.

6. REFERENCES

[1] E. Plenge, D. J. Poot, M. Bernsen, G. Kotek, G. Houston, P. Wielopolski, L. van der Weerd, W. J. Niessen, and E. Meijering, "Super-resolution methods in MRI: Can they improve the trade-off between resolution, signal-to-noise ratio, and acquisition time?," *Magnetic Resonance in Medicine*, vol. 68, no. 6, pp. 1983–1993, 2012.

[2] E. Van Reeth, I. K. Tham, C. H. Tan, and C. L. Poh, "Super-resolution in magnetic resonance imaging: A review," *Concepts in Magnetic Resonance Part A*, vol. 40A, no. 6, pp. 306–325, 2012.

[3] M. Delbany, A. Bustin, J. Poujol, I. Thomassin-Naggara, J. Felblinger, P.-A. Vuissoz, and F. Odille, "One-millimeter isotropic breast diffusion-weighted imaging: Evaluation of a superresolution strategy in terms of signal-to-noise ratio, sharpness and apparent diffusion coefficient," *Magnetic Resonance in Medicine*, vol. 81, no. 4, 2019.

[4] O. Oktay, W. Bai, M. Lee, R. Guerrero, K. Kamnitsas, J. Caballero, A. de Marvao, S. Cook, D. O'Regan, and D. Rueckert, "Multi-input Cardiac Image Super-Resolution Using Convolutional Neural Networks," in *Medical Image Computing and Computer-Assisted Intervention*, MICCAI 2016, Ed., Cham, 2016, Lecture Notes in Computer Science, pp. 246–254, Springer International Publishing.

[5] J. Shi, Z. Li, S. Ying, C. Wang, Q. Liu, Q. Zhang, and P. Yan, "MR Image Super-Resolution via Wide Residual Networks With Fixed Skip Connection," *IEEE Journal of Biomedical and Health Informatics*, vol. 23, no. 3, pp. 1129–1140, May 2019.

[6] A. Gholipour, J.A. Estroff, and S.K. Warfield, "Robust Super-Resolution Volume Reconstruction From Slice Acquisitions: Application to Fetal Brain MRI," *IEEE Transactions on Medical Imaging*, vol. 29, no. 10, pp. 1739–1758, Oct. 2010.

[7] H. Greenspan, G. Oz, N. Kiryati, and S. Peled, "MRI inter-slice reconstruction using super-resolution," *MAGNETIC RESONANCE IMAGING*, vol. 20, no. 5, pp. 437–446, June 2002.

[8] F. Odille, A. Bustin, B. Chen, P.-A. Vuissoz, and J. Felblinger, "Motion-corrected, super-resolution reconstruction for high-resolution 3d cardiac cine mri," in *International Conference on Medical Image Computing and Computer-Assisted Intervention*. Springer, 2015, pp. 435–442.

[9] F. Rousseau, O. Glenn, and C. Studholme, *A novel approach to high resolution fetal brain MR imaging*, vol. 3749 of *Lecture Notes in Computer Science*, Springer, Berlin New York London [etc.], 2005.

[10] X. Zhang, E. Y. Lam, E. X. Wu, and K. Y. Wong, "Application of Tikhonov Regularization to Super-Resolution Reconstruction of Brain MRI Images," in *Medical Imaging and Informatics*, Xiaohong Gao, Henning Müller, Martin J. Loomes, Richard Comley, and Shuqian Luo, Eds., number 4987 in Lecture Notes in Computer Science, pp. 51–56. Springer Berlin Heidelberg, 2008.

[11] S. Tourbier, X. Bresson, P. Hagmann, J.-P. Thiran, R. Meuli, and M. B. Cuadra, "Efficient total variation algorithm for fetal brain MRI reconstruction," *Medical image computing and computer-assisted intervention: MICCAI ... International Conference on Medical Image Computing and Computer-Assisted Intervention*, vol. 17, no. Pt 2, pp. 252–259, 2014.

[12] F. Shi, J. Cheng, L. Wang, P.-T. Yap, and D. Shen, "LRTV: MR Image Super-Resolution with Low-Rank and Total Variation Regularizations," *IEEE transactions on medical imaging*, vol. 34, no. 12, pp. 2459–2466, Dec. 2015.

[13] A. Bustin, D. Voilliot, A. Menini, J. Felblinger, C. de Chillou, D. Burschka, L. Bonnemains, and F. Odille, "Isotropic Reconstruction of MR Images Using 3D Patch-Based Self-Similarity Learning," *IEEE transactions on medical imaging*, vol. 37, no. 8, pp. 1932–1942, Aug. 2018.

[14] C. I. Kanatsoulis, X. Fu, N. D. Sidiropoulos, and W.-K. Ma, "Hyperspectral Super-Resolution: A Coupled Tensor Factorization Approach," *IEEE Trans. Signal Process.*, vol. 66, no. 24, pp. 6503–6517, 2018.

[15] C. Prévost, K. Usevich, P. Comon, and D. Brie, "Hyperspectral Super-Resolution with Coupled Tucker Approximation: Identifiability and SVD-based algorithms," *IEEE Trans. Signal Process.*, vol. 68, pp. 931–946, 2020.

[16] G. Zhang, X. Fu, J. Wang, X.-L. Zhao, and M. Hong, "Spectrum cartography via coupled block-term tensor decomposition," *IEEE Trans. Signal Process.*, 2020.

[17] B. Yaman, S. Weingärtner, N. Kargas, N. D. Sidiropoulos, and M. Akçakaya, "Low-rank tensor models for improved multidimensional mri: Application to dynamic cardiac t_1 mapping," *IEEE transactions on computational imaging*, vol. 6, pp. 194–207, 2019.

[18] C. I. Kanatsoulis, X. Fu, N. D. Sidiropoulos, and M. Akçakaya, "Tensor Completion from Regular Sub-Nyquist Samples," *arXiv e-prints*, p. arXiv:1903.00435, Mar. 2019.

[19] L. De Lathauwer, "Decompositions of a Higher-Order Tensor in Block Terms—Part II: Definitions and Uniqueness," *SIAM J. Matrix Anal. Appl.*, vol. 30, no. 3, pp. 1033–1066, 2008.

[20] P. Comon, "Tensors: A brief introduction," *IEEE Signal Process. Mag.*, vol. 31, no. 3, pp. 44–53, 2014.

[21] T. G. Kolda and B. W. Bader, "Tensor Decompositions and Applications," *SIAM Review*, vol. 51, no. 3, pp. 455–500, 2009.

[22] G. H. Golub, P. C. Hansen, and D. P. O'Leary, "Tikhonov regularization and total least squares," *SIAM journal on matrix analysis and applications*, vol. 21, no. 1, pp. 185–194, 1999.

[23] V. Simoncini, "Computational methods for linear matrix equations," *SIAM Review*, vol. 58, no. 3, pp. 377–441, 2016.

[24] N. Vervliet, O. Debals, L. Sorber, M. Van Barel, and L. De Lathauwer, *Tensorlab 3.0*, Available online, 2016.

[25] D. Zosso and A. Bustin, "A primal-dual projected gradient algorithm for efficient beltrami regularization," *Computer Vision and Image Understanding*, pp. 14–52, 2014.

[26] W. Pei, G. Wang, and X. Yu, "Performance evaluation of different references based image fusion quality metrics for quality assessment of remote sensing image fusion," in *2012 IEEE International Geoscience and Remote Sensing Symposium*. IEEE, 2012, pp. 2280–2283.

[27] G. Blanchet and L. Moisan, "An explicit sharpness index related to global phase coherence," in *2012 IEEE International Conference on Acoustics, Speech and Signal Processing (ICASSP)*. IEEE, 2012, pp. 1065–1068.